Thin Solid Films xxx (2016) xxx–xxx

Contents lists available at ScienceDirect

Thin Solid Films

journal homepage: www.elsevier.com/locate/tsf

WC/C:H films synthesized by an hybrid reactive magnetron sputtering/Plasma Enhanced Chemical Vapor Deposition process: An alternative to Cr (VI) based hard chromium plating

C. Nouvellon [a,*], R. Belchi [b], L. Libralesso [b], O. Douhéret [a], R. Lazzaroni [a,c], R. Snyders [a,d], D. Thiry [d]

[a] Materia Nova Research Center, Avenue Copernic 1, 7000 Mons, Belgium
[b] CRM group, allée de l'Innovation 1, B57, B-4000 Liège, Belgium
[c] Laboratory for Chemistry of Novel Materials, (CMN), CIRMAP, Université de Mons, 23 Place du Parc, 7000 Mons, Belgium
[d] Chimie des Interactions Plasma-Surface (ChIPS), CIRMAP, Université de Mons, 23 Place du Parc, 7000 Mons, Belgium

ARTICLE INFO

Article history:
Received 20 May 2016
Received in revised form 1 September 2016
Accepted 1 September 2016
Available online xxxx

Keywords:
Magnetron sputtering
Tungsten carbide
Amorphous carbon
Nanocomposites
Hardness
Friction
Wear
Thin film growth

ABSTRACT

WC/C:H thin films have been synthesized by a hybrid Plasma Enhanced Chemical Vapor Deposition/Physical Vapor Deposition method consisting in the reactive sputtering of a tungsten target in Ar-C_2H_2 atmospheres. The influence of the gas mixture on the physico-chemical properties of WC/C:H layers including their chemical composition, morphology, tribological and mechanical features has been studied.

X-ray photoelectron spectroscopy measurements reveal an increase in the carbon content and a higher aliphatic bonds density in detriment to the carbide ones as a function of the acetylene flow. These results, in combination with Raman spectroscopy, X-ray diffraction, transmission electron microscopy and atomic force microscopy data, allow to depict the material as crystallized W_xC_{1-y} nano-spheres (corresponding to aggregate of smaller nanograins of W_2C and WC_{1-x}) diluted in a hydrogenated carbon matrix; the ratio between the hard crystallized WC phase and the softer hydrogenated carbon matrix being reduced when increasing the acetylene flow.

The film nanohardness and tribological properties (i.e. friction coefficient and wear rate) are directly connected to the film chemical composition and structure. High nanohardness (~20 GPa), friction coefficient of $\mu = 0.5$ and high wear rate ($5.4 \cdot 10^{-13}$ m^2/N) are obtained for the lowest carbon content of 37 at.%. When increasing the carbon content in the film (77 at.%), the hardness strongly decreases to ~10 GPa and a lower friction coefficient ($\mu = 0.2$) and wear rate ($4.7 \cdot 10^{-15}$ m^2/N) are obtained. These properties are similar and even better than the ones of Cr(VI) based electroplating coatings, demonstrating the attractiveness of our WC/C:H films as a potential alternative to these coatings.

1. Introduction

Hard chromium plating is a process enabling the synthesis of hard chromium layer exhibiting very attractive properties such as a high wear and corrosion resistance as well as a low friction coefficient. All these features justify the use of this material in numerous industrial applications like in the aerospace, automotive, petrochemical fields and machinery components and tools (e.g. valves, hydraulics, pumps, stamping dies, and molds) [1].

However, the main drawback of this technology is the use of highly toxic and carcinogenic chromic (VI) acid baths [2]. Numerous efforts have therefore been devoted to the development of an alternative material with at least equal or even better properties than hard chromium.

Yet, it quickly appears to the scientists that for obtaining similar properties than hard chromium layer, a unique material cannot fulfill all the requirements. Therefore, the usual strategy consists in the fabrication of a nanocomposite coating composed of a matrix embedding nanoparticles of another material. The idea behind this approach is to positively combine the properties of both components (i.e. the matrix and the nanoparticles). The modulation of the physico-chemical properties of the material can be achieved by adjusting the chemical composition of the nanocomposite as well as the size and the density of the nanoparticles. In this context, nano-composites formed by Metal-Carbide nanoparticles embedded in a carbon (hydrogenated or not) matrix with the metal being Si [3] or a transition metal [4] such Mo, Nb, Ta, Cr, Ti and W [5,6,7,8,9] have attracted a considerable attention. Among these materials, carbon (hydrogenated or not)-based tungsten-carbide nanocomposite (WC/C or WC/C:H) appears as one of the most promising due to its high hardness, wear resistance [10], relatively low conductivity, excellent chemical stability [11] and a high corrosion resistance in

* Corresponding author.
E-mail address: corinne.nouvellon@materianova.be (C. Nouvellon).

http://dx.doi.org/10.1016/j.tsf.2016.09.002
0040-6090/

acidic media [12]. Furthermore, it has been reported that WC/C:H layers exhibit low internal stresses and reduced brittleness [13] promoting the adhesion of the layer to a given substrate.

Several synthesis methods including vacuum processes such as the combination of pulsed laser ablation and magnetron sputtering [13], the combination of RF reactive magnetron sputtering with plasma source ion implantation [14], the sputtering with a magnetron arc source [3] or co-sputtering of WC and C targets in Ar atmosphere [11] have been employed for the fabrication of these coatings. Among them, the hybrid PECVD ("Plasma Enhanced Chemical Vapor Deposition")/PVD ("Physical Vapor Deposition") technique involving the simultaneous sputtering of a tungsten target in a reactive hydrocarbon atmosphere such as C_2H_2 [3,15], CH_4 [16] or C_6H_6 [12,17] and the dissociation of organic molecules in the plasma giving rise to the inclusion of WC nanoparticles in a hydrogenated carbon matrix (WC/C:H) is of particular interest. Indeed, this approach combines significant advantages such as the absence of solvent making this technique compatible with the modern quest for environmentally friendly technology, a possible industrial up-scaling and a high flexibility enabling to tune in a wide range the properties of the material [18].

Here, we report on the study of the synthesis of WC/C:H coatings by a hybrid PECVD/reactive magnetron sputtering process in Ar/C_2H_2 gas mixture. At first, a thorough characterization of the physico-chemical (i.e. chemical composition, crystalline and mechanical properties, morphology) properties of the WC/C:H layers on Si substrates has been undertaken as a function of the amount of C_2H_2 in the discharge. In a second step, tribological (i.e. wear rate and friction coefficient) as well as mechanical (i.e. hardness) properties have been investigated for WC/C:H coatings deposited on steel substrates for optimized synthesis conditions. The performance of the WC/C:H coatings in comparison with an industrial reference, namely hard chrome layer formed by electroplating process, is discussed.

2. Experimental details

The coatings are deposited onto Si (low resistivity doped silicon wafers) and low alloy CrMo steel plates (4140 ASTM or EN 42CrMo4, containing 0.4% C, 1% Cr, 0.2% Mo, 0.25% Si and 0.8% Mn). Prior to their introduction in the chamber, steel substrates are chemically cleaned with Ridoline C75 alkaline solution at 60 °C. They are then in-situ etched by AC (40 kHz) Ar plasma at 10 Pa during 20 min.

The experiments are carried out in a semi-industrial TSD 400-CD (HEF R&D) coating chamber, pumped through a combination of a primary and turbomolecular pumps allowing to reach a residual pressure $<3 \cdot 10^{-4}$ Pa. A tungsten target (450 * 150 mm provided by Plansee) was sputtered in Ar/C_2H_2 gas mixture using an ENI RPG asymmetric bipolar pulsed DC power supply operating with a frequency of 250 kHz and a reverse pulse duration of 1616 ns. The mean sputtering power was fixed at 1000 W. The substrate holder connected to the ground was rotated at a speed of 5 rpm and located 9 cm in front of the cathode.

The total gas flow ($Ar + C_2H_2$) is fixed to 100 sccm. In our experimental window, the relative proportion of C_2H_2 in the gas mixture, i.e. X (C_2H_2), varies from 5% to 20%. During the process, the working pressure is unfixed and varies between 0.5 and 0.7 Pa depending on X (C_2H_2).

Prior to WC/C:H coating on steel, a 500 nm Cr layer is deposited in the same chamber by sputtering a Cr target (450 * 150 mm) at 2 kW in an Ar atmosphere in order to promote the adhesion.

The thickness of the films is measured by Dektak mechanical profilometer (Veeco, Dektak 150) performed on Si wafer, measuring the step between a coated and an uncoated zone. Films with a constant thickness of 400 nm have been deposited by adjusting the deposition time.

X-ray photoelectron spectroscopy (XPS) measurements are performed using a PHI 5000 VersaProbe apparatus by means of a mochromatized Al Kα radiation (1486.6 eV) as photon source. The atomic relative concentration of each element is calculated from peak areas taking into account the respective photoionization cross sections, the electron inelastic mean free path, and the transmission function of the spectrometer. Before analysis, the samples are submitted to an Ar^+ ion bombardment at 1 kV during 2 min to eliminate the surface pollution. Photoelectrons were collected at a takeoff angle of 45° from the surface normal. All spectra were charge corrected with respect to the hydrocarbon component of the *C*1 s peak at 285 eV. The XPS survey were acquired using a pass energy of 117.4 eV. Concerning the high-resolution peaks of each element, a pass energy of 23.5 eV was employed. For spectral curve fitting of the carbon photoelectron peak using PHI Multipak Software, a full width at half-maximum of 1–1.3 eV and a Gauss–Lorentz function (70–85% Gauss) were applied. The high-resolution *C*1s photoelectrons peaks were acquired with energy step of 0.2 eV. The XPS resolution of our apparatus is estimated to be 0.5 eV [19,20].

Raman spectra measurements (400–2000 cm^{-1}) were carried out in a Bruker Senterra spectrometer equipped with a CCD detector and a He-Ne laser (532 nm) at 10 mW.

The crystal structure of the films is examined by X-ray diffraction (XRD) analysis using Cu Kα radiation (1.54 Å) in a PANanalytical diffractometer in the θ-2θ configuration. Spectra are acquired in the 30–50° range with steps of 0.026°. Topographical analyses of the films are carried out with a Bruker multimode Atomic Force Microscopy (AFM) in tapping mode scanning configuration (TM-AFM) and equipped with a Nanoscope III controller and a phase extended module. Etched Si probe (PPP-NCHR Nanosensors GmbH) is used.

Transmission Electronic Microscope (TEM) analyses are carried out in a Philips CM200 microscope operating at 120 kV. The pictures are acquired with a CCD camera from Gatan (type Orius 600). 50 nm layers are deposited on copper grid coated with an amorphous carbon layer.

Nanoindentation experiments are performed at room temperature, using a G200 nanoindenter (MTS instrument, E1757) with a Berkovich type diamond indenter. The load displacement data are analyzed using the Oliver and Pharr method [21] to determine the hardness as a function of the displacement of the indenter. Each film is indented with a 6*6 matrix points, with a 50 μm space between indents. The sample hardness values are then obtained from the average of those deduced from the 36 indentations per samples with the standard deviation representing the error. Hardness values are measured at a penetration depth corresponding to 10% of the coating thickness in order to reduce the influence of the substrate.

Tribological parameters are measured with a CSM pin-on-disk tribometer using an alumina ball (6 mm diameter, sliding speed of 10 cm/s and 5 N of applied load in ambient air, 20 °C, 50% relative humidity, 2000 laps, acquisition rate 5 Hz). The radius of the groove is 10 mm. The wear rate (m^2/N) corresponds to the loss of volume over the applied force and the length of the sliding. The loss of volume is determined by mechanical profilometry, measuring the depth and the width of the groove, at four equidistant sections.

3. Results and discussion

As already mentioned, in order to identify an adequate experimental window to optimize the mechanical and tribological properties of the coatings, the physico-chemical properties of the layers are first evaluated on Si substrates for facilitating the surface analysis methods. Then, for identified synthesis conditions, depositions are performed on 4140 steel substrates.

3.1. WC/C:H coatings on Si substrates

Fig. 1 shows the evolution of the elemental chemical composition of the coatings as a function of X (C_2H_2). It should be noted that the XPS spectra are recorded after sputtering the surface with Ar ions during 2 min in order to remove the surface pollution occurring during the storage of the samples in the air before analysis.

Please cite this article as: C. Nouvellon, et al., WC/C:H films synthesized by an hybrid reactive magnetron sputtering/Plasma Enhanced Chemical Vapor Deposition process: An alternat..., Thin Solid Films (2016), http://dx.doi.org/10.1016/j.tsf.2016.09.002

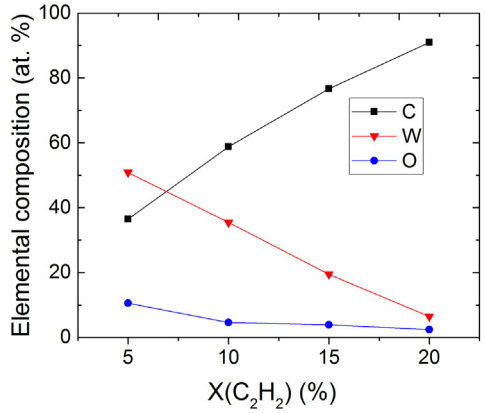

Fig. 1. Elemental chemical composition of the WC/C:H films as determined by XPS as a function of X (C_2H_2).

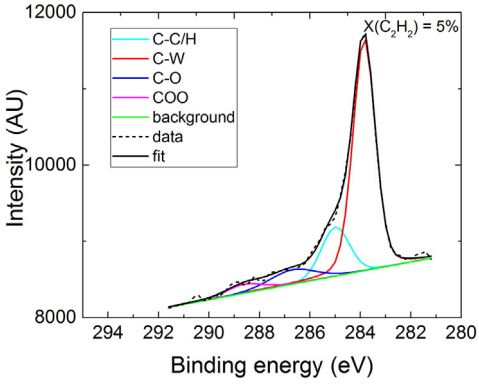

Fig. 2. Fitting of the C1s photoelectron peak for a WC/C:H coating deposited for X(C_2H_2) = 5%.

The atomic carbon content linearly increases (from ~37 to 91 at.%) with X (C_2H_2) whereas the atomic W content follows a reverse trend (from ~50 to ~7 at.%). Oxygen is also identified and decreases from 11 at.% to 2 at.% with X (C_2H_2). Its presence is attributed to the residual water in the deposition chamber and the oxidation of the material during its storage in the air before analysis. Both carbon-based species and tungsten can be oxidized forming C-OR/COOR and WO_3 (data not shown), respectively. Due to the higher oxygen uptake during the oxidation reaction of tungsten, the oxygen content follows the same trend as the atomic W concentration. It should be emphasized that regarding the oxidation occurring after the synthesis of the samples, the kinetic of the reaction is limited by the diffusion of the oxygen molecule in the material resulting in an enrichment of the surface by oxygen. This is confirmed by the evolution of the atomic oxygen concentration with the sputtering time (see Table 1 for the film synthesized at X (C_2H_2) = 20%) revealing the decrease in the oxygen content before reaching a stable value.

In order to assess the nature of the chemical bonding in the material, high C1s carbon resolution peaks are examined. Four components are used for the fitting procedure: two major peaks, namely C—W (283.9 eV) and C—C/H (285 eV) and two minor components ascribed to oxygen contamination (i.e. C—O and COO at 286.7 and 288.6 eV, respectively). An example of a spectral curve fitting of C1s envelope for X (C_2H_2) = 5% is depicted in Fig. 2. The analysis of Fig. 3 reveals the increase in the C—C/H bond in the material in detriment of the C—W component when increasing X (C_2H_2).

The evolution of the chemical composition of the coatings with X (C_2H_2) can be explained as follows. Actually, two different processes contribute to the growth of the layer, namely the reactive magnetron sputtering and the PECVD processes [22]. The former involves the condensation of W/C sputtered particles at the substrate. In fact, owing to the great affinity between carbon and tungsten [4], carbon-based species react at the W target surface forming a W/C compound, as confirmed by the evolution of the target voltage with X (C_2H_2). As depicted in Fig. 4, a small addition of C_2H_2 in the discharge (i.e. X (C_2H_2) = 5%) induces a significant increase in the target voltage (from 280 to 345 V) indicating a variation in the chemical state of the target by the formation of a WC compound which in turn affects the secondary electron emission yield of the target surface [23]. For further increase in X (C_2H_2), the target voltage remains almost constant implying that in our experimental window, the chemical state of the target remains practically unchanged. The variation of the target voltage can also be related to the modification of the chemical nature of the ions bombarding the cathode. Indeed, increasing X (C_2H_2) reduces the proportion of Ar ions in comparison to carbon-based ions in the ionic flux impinging the target. This could also influence the secondary electron emission yield and hence the target voltage. However, since the target voltage remains almost constant for X (C_2H_2) > 5%, the variation of the chemical state of the target surface is probably the prominent factor.

On the other hand, the PECVD contribution in the overall process arises from the condensation at the substrate surface of reactive carbon-based species coming from the electron-induced dissociation of C_2H_2 molecules in the plasma. The simultaneous occurrence of both processes (i.e. reactive magnetron sputtering and PECVD) leads, in fine, to a material containing C—W and C—C/H bonds, as determined by XPS. The chemical composition of the layers is therefore directly affected by the contribution of each process in the overall growth mechanism which depends on X (C_2H_2). At low X (C_2H_2), the process mainly operates in reactive magnetron sputtering mode since only 7% of C—C/H bonds is measured. When increasing X (C_2H_2) and in turn the concentration of carbon-based film-forming species, the PECVD part to the condensing flow of matter becomes more and more important resulting in a higher proportion of C—C/H bonds in the material. Furthermore, it has to be mentioned that the sputtering yield of the WC target by carbon-based ions is reduced in comparison to Ar bombarding ions, decreasing the contribution of the sputtering of the target in the formation of the C/W—C:H material. For X (C_2H_2) = 20%, the method

Table 1
Evolution of the atomic carbon, tungsten and oxygen content as a function of the sputtering time (Argon ions, 1 kV) in the coating synthesized for X (C_2H_2) = 20%.

Sputtering time (min)	C1s (at.%)	W4f (at.%)	O1s (at.%)
0	84	4	12
2	91	6	2
4	90	7	2
6	89	7	3

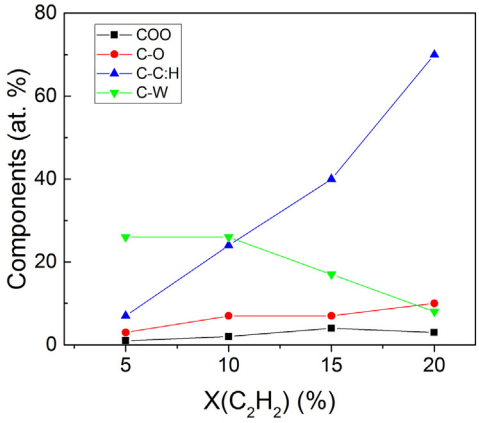

Fig. 3. Evolution of the carbon bonding with X(C_2H_2) in WC/C:H coatings.

Please cite this article as: C. Nouvellon, et al., WC/C:H films synthesized by an hybrid reactive magnetron sputtering/Plasma Enhanced Chemical Vapor Deposition process: An alternat..., Thin Solid Films (2016), http://dx.doi.org/10.1016/j.tsf.2016.09.002

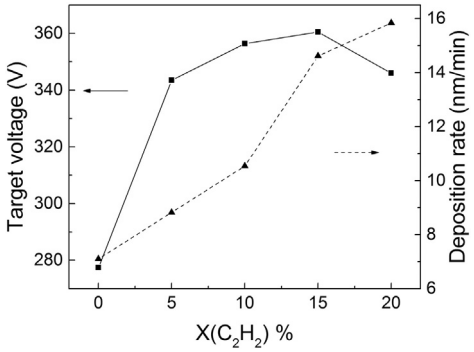

Fig. 4. Evolution of the W target voltage and the deposition rate as a function of $X(C_2H_2)$.

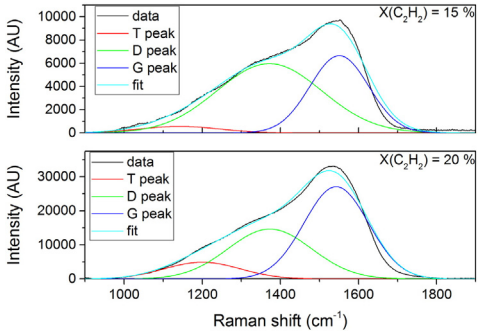

Fig. 6. Raman peak fitting spectra of the WC/C:H coatings synthesized for $X(C_2H_2) = 15$ and 20%.

can be viewed as mainly a PECVD-like technique since only 7 at.% W is measured.

The previous explanations are supported by the increase in the deposition rate with X (C_2H_2) (Fig. 4) due to the production of a higher concentration of carbon-based reactive species through electron-induced dissociations reactions.

To complete the description of the chemical properties of the material, Raman spectroscopy measurements have been carried out. The formation of an a-C:H phase (amorphous hydrogenated carbon based matrix) is evidenced by the presence of the two well-known D (i.e. breathing mode of the sp^2 sites in rings at 1370–1380 cm^{-1}) and G (stretching of all sp^2 sites at 1545–1550 cm^{-1}) peaks (Fig. 5) [24]. The overall intensity of the Raman signal increases with X (C_2H_2) since more carbon-based species is incorporated in the growing film as confirmed by XPS. It can be qualitatively observed that the intensity of the D peak in the global signal decreases with X (C_2H_2). This is further confirmed by deconvoluting the envelope for X (C_2H_2) = 15 and 20% (Fig. 6). It should be noted that the intensity of the signals for X (C_2H_2) < 15% is too low for enabling an accurate spectral curve fitting. Three Gaussian curves corresponding to the D and G peaks and an additional one attributed to the T peak indicating the presence of carbon atoms with sp^3 hybridization have been used for the fitting procedure [25]. When $X(C_2H_2)$ increases from 15 to 20%, we can simultaneously observe a small down shift of the G peak position from 1551 to 1543 cm^{-1} and a decrease in the I_D/I_G ratio from 1.6 to 0.7 which, according to Makowka et al. [25], can be ascribed to an increase in the hydrogen content in the carbon-based matrix. On the other hand, the proportional increase in the T peak when varying X (C_2H_2) from 15 to 20% reveals the increase in the proportion of carbon in sp^3 hybridization (Fig. 6). The more pronounced hydrogenation of the carbon-based matrix is therefore accompanied with the conversion of the sp^2 sites into sp^3 configuration.

The increase in the hydrogen concentration in the hydrogenated carbon-based matrix with X (C_2H_2) might be tentatively explained considering the influence of the gas mixture on the electron density of the plasma. It has been extensively reported that an increase in the Ar proportion in a gas mixture containing a molecule results in an increase in the electron density [26]. Therefore, a decrease in X (C_2H_2) is accompanied by an increase in the ion flux bombarding the growing film thus promoting the dehydrogenation reactions which occur at the interface. [22].

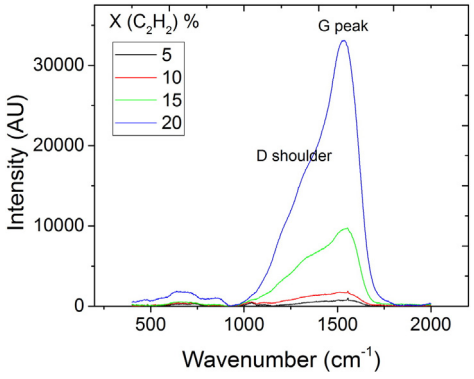

Fig. 5. Raman spectra of the WC/C:H coatings as a function of $X(C_2H_2)$.

From the XPS and Raman spectroscopies, it can be supposed that the WC/C:H material is formed by an hydrogenated carbon-based matrix in which W_xC_{1-y} particles are embedded. To investigate the organization of the material at the nanoscale, AFM measurements were performed.

Fig. 7 (a) and (b) display the height and phase TM-AFM images of the films synthesized for $X(C_2H_2)$ = 5% and 15%, respectively. The roughness (i.e. root mean square value) was found to decrease from 3.9 nm to 2.3 nm when varying X (C_2H_2) from 5 to 15%. For both conditions, the height images exhibit grain like features. The grains themselves appear to be composed of smaller grain aggregates. These aggregates can further be observed in the phase images. In tapping-mode AFM, the phase signal is both depending on the error amplitude signal (i.e. the reactivity of the electronic feedback of the detection system) and the mechanical properties of the different materials composing the film. Providing adjusted feedback, the error is minimized and the phase contrast only refers to the difference of mechanical properties between the two materials forming the composite. In our case, as no cross-talking is actually observed between the height and phase signals, this indicates that the contribution of the error signal in the phase contrast can be neglected. Hence, bright features are supposed to correspond to one material and the dark ones to the other one. As the phase signal is merely qualitative, no direct correlation between phase values and material hardness can be done. Yet, as the phase contrasts seems to delineate bright features within a dark background, it suggests that the dark contrast might correspond to the hydrogenated carbon matrix phase of the composite material. Furthermore, Fig. 7 (a) and (b) display two peaks like distribution of the phase signal. The peak corresponding to the maximum phase signal values relatively decreases when changing $X(C_2H_2)$ from 5 to 15%. This further supports the attribution of the highest phase signal to W_xC_{1-y}. It is therefore reasonable to attribute the bright features in the phase contrast to W_xC_{1-y} clusters protruding at the surface of a hydrogenated carbon matrix exhibiting henceforth low phase signal. For $X(C_2H_2)$ = 5%, a 1:1 surface ratio between the two phase distribution is observed. Increasing $X(C_2H_2)$ to 15% leads to 2:3 W_xC_{1-y} hydrogenated carbon rich surface ratio. As TM-AFM is only probing topographical properties, only the W_xC_{1-y} protruding at the surface can be observed. Hence, the phase signal distributions showing variations of ratio of bright features in a matrix cannot be quantitatively correlated to the variations of ratio of W_xC_{1-y} in the hydrogenated carbon matrix. Yet, this observation is qualitatively in good agreement with what reported from XPS and Raman characterization and confirm the increase in the hydrogenated carbon rich phase in the film with $X(C_2H_2)$. On the other hand, the phase profiles for both

Please cite this article as: C. Nouvellon, et al., WC/C:H films synthesized by an hybrid reactive magnetron sputtering/Plasma Enhanced Chemical Vapor Deposition process: An alternat..., Thin Solid Films (2016), http://dx.doi.org/10.1016/j.tsf.2016.09.002

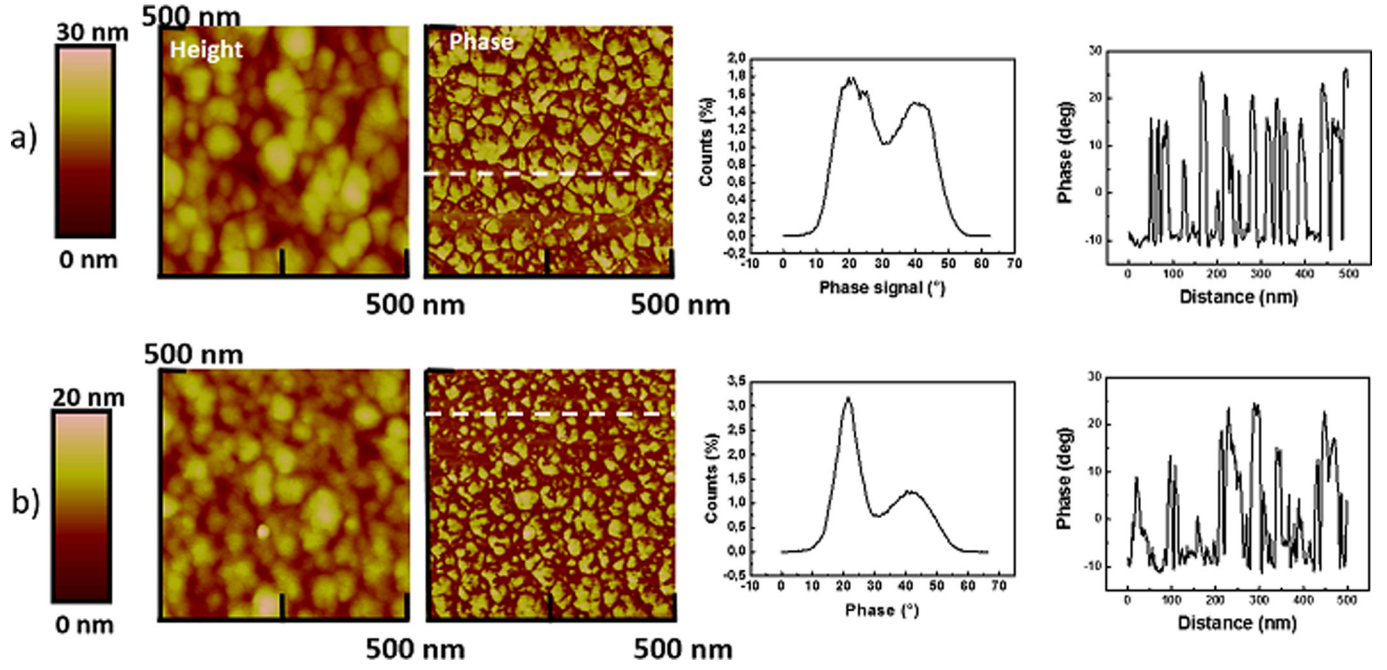

Fig. 7. AFM images (height and phase) and corresponding phase histograms and phase profiles (dash white line on phase image) of the WC/C:H coatings synthesized for X(C_2H_2) = a) 5 and b) 15%.

conditions are also depicted and reveal the presence of grains in the range 10–20 nm.

All these observations are supported by the TEM images recorded on films synthesized on copper grid for similar experimental conditions (Fig. 8). The dark domains (~15 nm in size) correspond to W_xC_{1-y} nanoparticles whereas the bright ones are ascribed to the hydrogenated carbon-based matrix. As unambiguously observed, the proportion of bright domains (i.e. the hydrocarbon-based matrix) in the TEM images increases with X (C_2H_2).

In order to study the crystalline structure of the material, XRD measurements were carried out (Fig. 9). For X (C_2H_2) > 10%, no diffraction peaks are detected meaning that the amount of crystallized grains is likely too low in comparison to the detection limit of the machine for enabling their detection. For X (C_2H_2) ≤ 10%, a broad peak centered at ~36.9° is identified; the intensity of the peak being more intense when decreasing X (C_2H_2). For better interpretation, this peak has been fitted (for X (C_2H_2) = 5%) with four Gaussian components after background subtraction and removal of Si peaks (Fig. 10). Since the α WC phase is usually not observed in WC films [11,17], the main peak at 36.5° is attributed to the (111) β WC_{1-x} cubic phase with a 0.4° lower angle shift which could indicate compressive stress in the material [27]. The second and third peaks are respectively associated to (002) and (101) planes of the W_2C phase. The fourth peak is difficult to attribute. From the XRD database, the only possibility is the (200) plane of the βWC_{1-x} phase with a large shift of around 2°. This could be explained by the presence of local stress within the material due to the lattice mismatch between the different crystallographic phases amplifying the shift in position [28]. Therefore, the observed large XRD peak could be attributed to a mixture of β WC_{1-x} cubic and W_2C hexagonal phases, as sub-stoichiometric composition has been measured by XPS. By means of the Scherrer's formula, the crystallite size is estimated from each individual component to be between 3 and 7 nm. Therefore, the grains observed in the AFM and TEM images with a diameter typically ranging from 10 to 20 nm are likely formed by smaller crystallized grains (i.e. 3–7 nm) of two different phases: W_2C and βWC_{1-x}.

Since the hardness is one of the most important criteria defining the performance of the WC/C:H layer, nanoindentation measurements are carried out. The results reveal a decrease in the nanohardness from 20

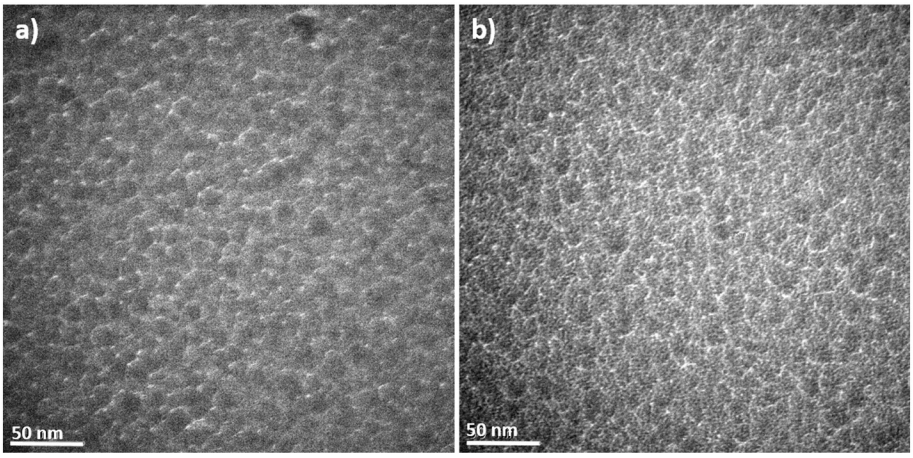

Fig. 8. Planar-view TEM micrograph of WC/C:H coatings synthesized for X(C_2H_2) = a) 5% and b) 15%.

Please cite this article as: C. Nouvellon, et al., WC/C:H films synthesized by an hybrid reactive magnetron sputtering/Plasma Enhanced Chemical Vapor Deposition process: An alternat..., Thin Solid Films (2016), http://dx.doi.org/10.1016/j.tsf.2016.09.002

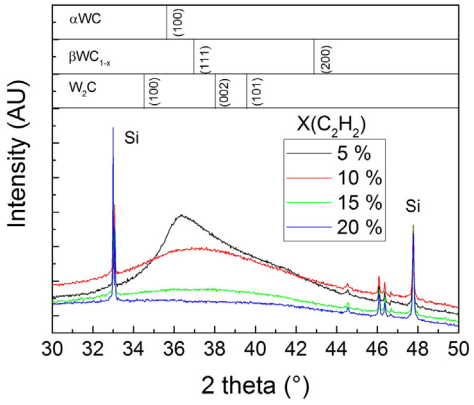

Fig. 9. XRD patterns of the WC/C:H coatings as a function of $X(C_2H_2)$.

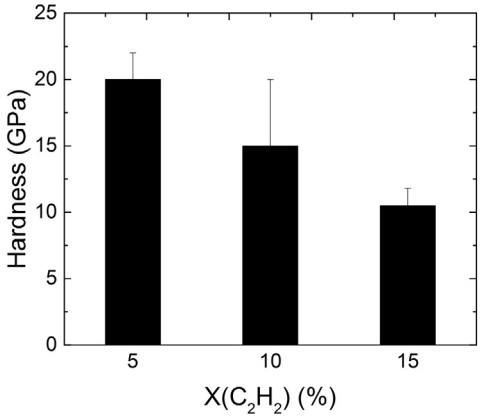

Fig. 11. Hardness of WC/C:H coatings as a function of $X(C_2H_2)$.

to 10.5 GPa when increasing X (C_2H_2) in the range 5–15%. Actually, based on all collected data, the concentration of W_xC_{1-y} grains including WC_{1-x} and W_2C phases embedded in the hydrogenated carbon matrix was found to decrease with X (C_2H_2). Since the W_xC_{1-y} phase is harder than the carbon hydrogenated one, the hardness is therefore expected to decrease with X (C_2H_2) in agreement with the data in Fig. 11. This conclusion also correlates with the contrast observed in the AFM images recorded in phase mode. It should be noted that an increase in the hydrogen concentration in the carbon-based matrix might also contribute to the decrease in the hardness with X (C_2H_2).

3.2. WC/C:H coatings on 4140 steel substrates

In view of the potential application of these coatings on steel, a similar deposition procedure is applied on 4140 steel substrates. Considering industrial applications including the improvement of wear-resistance of cutting and forming tools, besides the significance of tailoring the hardness of the protective layer, the wear rate properties as well as the friction coefficient are also of great interest. In this context, all these properties have been measured for WC/C:H coatings deposited on 4140 steel substrates for two extreme selected conditions (i.e. X (C_2H_2) = 5 and 15%). The data are summarized in Table 2 and compared to an industrial reference made of a 5 μm thick hard chromium electroplating layer deposited on the same steel substrate and to data extracted from the literature for comparable compounds deposited by magnetron co-sputtering process using WC/graphite targets [11] and W target arc sputtering in Ar/C_2H_2 mixtures [29]. For both WC/C:H layers, the hardness is higher than for the industrial Cr reference and is found to decrease from 18.5 to 12.5 GPa when increasing X (C_2H_2), in agreement with the measurements on Si substrate revealing the reproducibility of our process and the none influence of the substrate on the mechanical properties of the material. Furthermore, the measured hardness is in the same range as in other reported works [11,29]. On the other hand, with regard to the tribological properties (i.e. wear rate and friction coefficient), the layer synthesized for X (C_2H_2) = 15% exhibits the most attractive properties with the lowest friction coefficient (0.2) and wear rate ($4.7 \cdot 10^{-15}$ m^2/N). The decrease in the friction coefficient with X (C_2H_2) is correlated with the increase in the hydrogen proportion in the carbon-based matrix as deduced from the Raman spectroscopy. Regarding the wear rate, it is generally accepted that it follows the same trend than the hardness as also observed in this work [11,25].

The obtained results highlight the attractiveness of the optimized process to grow WC/C:H coatings with modulated hardness and tribological properties.

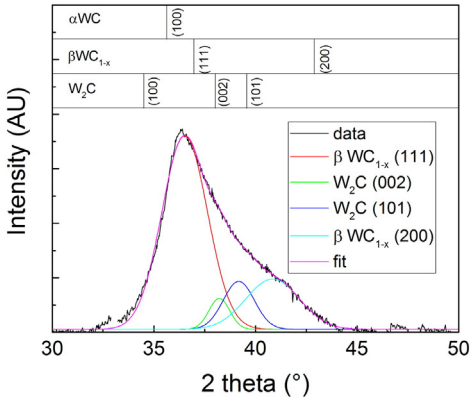

Fig. 10. XRD peak fitting of the WC/C:H coating synthesized for $X(C_2H_2) = 5\%$.

4. Conclusions

In this work, the synthesis of WC/C:H coatings by an hybrid PECVD/reactive magnetron sputtering process in Ar/C_2H_2 atmospheres is studied. It is shown that the physico-chemical properties of the nanocomposites, including their morphology, crystallinity as well as their chemical composition can be adjusted in a wide range by varying the proportion of C_2H_2 in the gas mixture. Ultimately, these features define the functional properties of the coatings such as the hardness or the friction coefficient making the process very attractive in view of the fabrication of tailor-made layers.

Our data reveal that the coatings deposited for low $X(C_2H_2)$ are sub stoichiometric with a high fraction of W—C bond. W_xC_{1-y} inclusions (from 10 to 20 nm) in the carbon-based matrix likely correspond to aggregate of smaller crystalline WC_{1-x} and W_2C nano grains of a few nanometers in diameter. The highest hardness value is obtained for this coating because of the harder W_xC_{1-y} phase in comparison with the hydrogenated carbon matrix. When increasing the acetylene flow, the carbon content and the aliphatic bonds density increase in expense of the C—W component. This induces a decrease in hardness but also a

Table 2
Mechanical and tribological properties of WC/C:H coatings on 4140 steel compared to an industrial reference of 5 μm hard chromium electroplating coating and to data extracted from the literature for comparable compounds.

Sample reference	Nano hardness (GPa)	friction coefficient μ	Wear rate (m^2/N)
$X(C_2H_2) = 5\%$	18.5	0.5	$5.4 \cdot 10^{-13}$
$X(C_2H_2) = 15\%$	12.5	0.2	$4.7 \cdot 10^{-15}$
Hard chromium	10	0.7	$1.0 \cdot 10^{-13}$
WC/C co-sputtering	16	0.2	
[9]	36	0.8	
W arc in Ar/C_2H_2 [24]	15	<0.1	
	32	>0.6	

Please cite this article as: C. Nouvellon, et al., WC/C:H films synthesized by an hybrid reactive magnetron sputtering/Plasma Enhanced Chemical Vapor Deposition process: An alternat..., Thin Solid Films (2016), http://dx.doi.org/10.1016/j.tsf.2016.09.002

lower friction coefficient and wear rate, when deposited on 4140 steel substrates.

Since our "best" coating exhibits better tribological and mechanical properties than an industrial hard Cr layer formed by electroplating, we have demonstrated the attractiveness of the hybrid PECVD/reactive magnetron sputtering method to grow WC/C:H layers as an efficient and "green" alternative to the chromium electroplating technique paving the way for industrial applications in the tool protection area.

Acknowledgments

This work is supported by the Department of the Research Programs (1317996) of the DGO6 (Wallonia) within the framework of Cornet program under the name of AlTi2De project. D. Thiry and R. Snyders acknowledge the support of the Belgian Government (Belspo) through the "Pôle d'attraction interuniversitaire" (PAI, P07/14, "Plasma-Surface Interaction"). The authors would like to thank Plansee for providing the W target, L. Szparaga and Pr J. Ratjski (University of Koszalin-Poland) for steel sample grinding, A. Roobroeck, Y. Paint and S. Deprez (Materia Nova R&D) for XPS, TEM and Raman measurements and M. Raza (University of Mons) for XRD analysis.

References

[1] K.O. Legg, M. Graham, P. Chang, F. Rastagar, A. Gonzales, B. Sartwell, The replacement of electroplating, Surf. Coat. Technol. 81 (1996) 99.
[2] L. Maria Irudaya Raj, J. Sathishkumar, B. Kumaragurubaran, P. Gopal, Analysis of hard chromium coating defects and its prevention methods, Int. J. Eng. Adv. Technol. 2 (5) (2013) 427.
[3] W. Precht, A. Czyzniewski, Deposition and some properties of carbide/amorphous carbon nanocomposites for tribological application, Surf. Coat. Technol. 174–175 (2003) 979.
[4] U. Jansson, E. Lewin, Sputter deposition of transition-metal carbide films — a critical review from a chemical perspective, Thin Solid Films 536 (2013) 1.
[5] R. Sanjinés, M.D. Abad, C. Vâju, R. Smajda, M. Mionić, A. Magrez, Electrical properties and applications of carbon based nanocomposite materials: an overview, Surf. Coat. Technol. 206 (2011) 727–733.
[6] G. Ma, S. Gong, G. Lin, L. Zhang, G. Sun, A study of structure and properties of Ti-doped DLC film by reactive magnetron sputtering with ion implantation, Appl. Surf. Sci. 258 (2012) 3045.
[7] C.W. Zou, H.J. Wang, L. Feng, S.W. Xue, Effects of Cr concentrations on the microstructure, hardness, and temperature-dependent tribological properties of Cr-DLC coatings, Appl. Surf. Sci. 286 (2013) 137.
[8] C. Corbella, E. Bertran, M.C. Polo, E. Pascual, J.L. Andújar, Structural effects of nanocomposite films of amorphous carbon and metal deposited by pulsed-DC reactive magnetron sputtering, Diam. Relat. Mater. 16 (2007) 1828.
[9] K. Bewilogua, C.V. Cooper, C. Specht, J. Schroder, R. Wittorf, M. Grischke, Erratum to: "Effect of target material on deposition and properties of metal-containing DLC (Me-DLC) coatings", Surf. Coat. Technol. 132 (2000) 275.
[10] B. Mahmoudi, G.L. Doll, C.H. Hager Jr., R.D. Evans, Influence of a WC/a-C:H tribological coating on micropitting wear of bearing steel, Wear 350-351 (2016) 107.
[11] M.D. Abad, M.A. Muñoz-Márquez, S. El Mrabet, A. Justo, J.C. Sánchez-López, Tailored synthesis of nanostructured WC/a-C coatings by dual magnetron sputtering, Surf. Coat. Technol. 204 (2010) 3490.
[12] P. Dubcek, N. Radic, O. Milat, S. Bernstorf, Grazing incidence small angle X-ray scattering investigation of tungsten–carbon films produced by reactive magnetron sputtering, Surf. Coat. Technol. 151-152 (2002) 218.
[13] A.A. Voevodin, J.P. O'Neill, J.S. Zabinski, Tribological performance and tribochemistry of nanocrystalline WC/amorphous diamond-like carbon composites, Thin Solid Films 342 (1999) 194.
[14] K. Baba, R. Hatada, Deposition and characterization of Ti- and W-containing diamond-like carbon films by plasma source ion implantation, Surf. Coat. Technol. 169-170 (2003) 287.
[15] C. Strondl, N.M. Carvalho, J.T.M. De Hosson, T.G. Krug, Influence of energetic ion bombardment on W-C:H coatings deposited with W and WC targets, Surf. Coat. Technol. 200 (2005) 1142.
[16] C. Rincon, J. Romero, J. Esteve, E. Martinez, A. Lousa, Effects of carbon incorporation in tungsten carbide films deposited by r.f. magnetron sputtering: single layers and multilayers, Surf. Coat. Technol. 163–164 (2003) 386.
[17] N. Radic, B. Grzeta, O. Milat, J. Ivkov, M. Stubicar, Tungsten–carbon films prepared by reactive sputtering from argon–benzene discharges, Thin Solid Films 320 (1998) 192.
[18] D. Thiry, S. Konstantinidis, J. Cornil, R. Snyders, Plasma diagnostics for the low-pressure plasma polymerization process: a critical review, Thin Solid Films 606 (2016) 19.
[19] D. Thiry, R. Francq, D. Cossement, D. Guerin, D. Vuillaume, R. Snyders, Establishment of a derivatization method to quantify thiol function in sulfur-containing plasma polymer films, Langmuir 29 (2013) 13183.
[20] S. Ligot, F. Renaux, L. Denis, D. Cossement, N. Nuns, P. Dubois, R. Snyders, Experimental study of the plasma polymerization of ethyl lactate, Plasma Process. Polym. 11 (2013) 999.
[21] W.C. Oliver, G.M. Pharr, An improved technique for determining hardness and elastic modulus using load and displacement sensing indentation experiments, J. Mat. Res. 7 (1992) 1564.
[22] D. Thiry, A. De Vreese, F. Renaux, J.L. Colaux, S. Lucas, Y. Guinet, L. Paccou, E. Bousser, R. Snyders, Toward a better understanding of the influence of the hydrocarbon precursor on the mechanical properties of a-C:H coatings synthesized by a hybrid PECVD/PVD method, Plasma Process. Polym. 13 (2016) 316.
[23] D. Depla, S. Heirwegh, S. Mahieu, J. Haemers, R. De Gryse, Understanding the discharge voltage behavior during reactive sputtering of oxides, J. Appl. Phys. 100 (1) (2007) 013301.
[24] J. Robertson, Diamond like amorphous carbon, Mater. Sci. Eng. R 37 (2002) 129.
[25] M. Makowka, W. Pawlak, P. Konarski, B. Wendler, Hydrogen content influence on tribological properties of nc-WC/a-C:H coatings, Diam. Relat. Mater. 67 (2016) 16.
[26] J.T. Gudmundsson, T. Kimura, M.A. Lieberman, Plasma sources, Sci. Technol. 8 (1999) 22.
[27] C.D. Rivera-Tello, E. Broitman, F.J. Flores-Ruiz, O. Jimenez, M. Flores, Mechanical properties and tribological behavior at micro and macro-scale of WC/WCN/W hierarchical multilayer coatings, Trib. Int. 101 (2016) 194.
[28] A.A. El Mel, F. Boukli-Hacene, L. Molina-Luna, N. Bouts, A. Chauvin, D. Thiry, E. Gautron, N. Gautier, P.-Y. Tessier, Unusual dealloying effect in gold/copper alloy thin films: the role of defects and column boundaries in the formation of nanoporous gold, ACS Appl. Mater. Interfaces 7 (4) (2015) 2310.
[29] A. Czyzniewski, Deposition and some properties of nanocrystalline WC and nanocomposite WC/a-C:H coatings, Thin Solid Films 433 (2003) 180.

Please cite this article as: C. Nouvellon, et al., WC/C:H films synthesized by an hybrid reactive magnetron sputtering/Plasma Enhanced Chemical Vapor Deposition process: An alternat..., Thin Solid Films (2016), http://dx.doi.org/10.1016/j.tsf.2016.09.002